Materials Horizons

Superprotonic Conductivity in $RbH_{2-3y}(PO_4)_{1-y}$: a Phosphate Deficient Analog to Cubic CsH_2PO_4 in the $(1-x)RbH_2PO_4 - xRb_2HPO_4$ System

Journal:	*Materials Horizons*
Manuscript ID	MH-COM-06-2023-000852.R2
Article Type:	Communication
Date Submitted by the Author:	22-Sep-2023
Complete List of Authors:	Xiong, Grace; Northwestern University, Materials Science and Engineering Wang, Louis; Northwestern University, Materials Science and Engineering Haile, Sossina; Northwestern University, Materials Science and Engineering

Creation of novel proton-conducting electrolytes with a combination of desirable properties, including negligible electronic conductivity, chemical stability, and processability, has taken on increased urgency as the world turns to hydrogen as a clean energy carrier. Superprotonic solid acids, in particular phosphates in this group, hold technological potential as components in fuel cells and other electrochemical devices. In such materials, orientational disorder of polyanion groups in high temperature phases facilitates rapid proton transport. Traditional chemical modification routes, such as replacing Cs^+ with Rb^+ to influence proton mobility or replacing $(HPO_4)^{2-}$ with $(SO_4)^-$ to influence both mobility and carrier concentrations, so as to support high conductivity at reduced temperatures, have been exhausted without generating technologically relevant outcomes. Here we show, using RbH_2PO_4 as an example, that the superprotonic phase can be stabilized to reduced temperatures by decreasing the $Rb:PO_4$ ratio. Remarkably, the cubic phase can support a large concentration of anion vacancies with stoichiometry described according to $RbH_{2-3y}(PO_4)_{1-y}$. Thus, anion deficiency emerges as a new approach to designing superprotonic electrolytes, complimenting very recent and less surprising demonstrations of cation deficient analogs.

Superprotonic Conductivity in $RbH_{2-3y}(PO_4)_{1-y}$: a Phosphate Deficient Analog to Cubic CsH_2PO_4 in the $(1-x)RbH_2PO_4 - xRb_2HPO_4$ System

Grace Xiong, Louis S. Wang, and Sossina M. Haile

Department of Materials Science and Engineering, Northwestern University, Evanston, IL 60208

Abstract

In contrast to CsH_2PO_4 (cesium dihydrogen phosphate, CDP), a material with a well-established superprotonic transition to a high conductivity state at 228°C, RbH_2PO_4 (rubidium dihydrogen phosphate, RDP) decomposes upon heating under ambient pressure conditions. Here we find, from study of the $(1-x)RbH_2PO_4 - xRb_2HPO_4$ system, the remarkable occurrence of cubic, off-stoichiometric $RbH_{2-3y}(PO_4)_{1-y}$, or α-RDP, with a variable $Rb:PO_4$ ratio. Materials were characterized by simultaneous thermal analysis and in situ X-ray powder diffraction performed under high steam partial pressure, from which the phase diagram between RbH_2PO_4 ($x = 0$) and $Rb_5H_7(PO_4)_4$ ($x = ¼$) was established. The system displays eutectoid behavior, with a eutectoid transition temperature of 242.0±0.5 °C and eutectoid composition of $x = 0.190 \pm 0.004$. Even the end-member $Rb_5H_7(PO_4)_4$ appears to transform to α-RDP, implying y in the chemical formula of 0.2 and a phosphate site vacancy concentration as high as 20%. Charge balance is attained by a decrease in the average number of protons on the remaining phosphate groups. The cubic lattice parameter at $x = 0.180$, near the eutectoid composition, and at a temperature of 249 °C is 4.7138(2) Å. This value is substantially smaller than the estimated ambient-pressure lattice parameter of stoichiometric RbH_2PO_4 of 4.837(12) Å, consistent with the proposal of phosphate site vacancies in the former. The superprotonic conductivity of the $x = 0.180$ material is 6×10^{-3} S/cm at 244°C, a factor of three lower than that of CDP at the same temperature. While the engineering properties of α-RDP do not suggest immediate technological relevance, the discovery of a superprotonic solid acid with a high concentration of phosphate site vacancies opens new avenues for developing proton conducting electrolytes, and in particular, for controlling their transition behavior.

Introduction

Superprotonic solid acids are materials in which high proton conductivity results from high levels of structural disorder within an otherwise crystalline framework.[1] In such materials, proton-bearing polyanion groups undergo rapid reorientations, which, along with proton transfer between the anion groups, facilitate long-range proton motion. Typically, the disordered superprotonic phase emerges upon heating to moderate temperatures (100 – 250° C). Amongst materials in this class, CsH_2PO_4 has received the greatest attention for potential technological applications because of its chemical stability under both oxidizing and reducing conditions.[2-9] Sulfate and selenate superprotonic compounds, of which many are known (including $CsHSO_4$[10] and $Rb_3H(SeO_4)_2$[11], and even mixed sulfate-phosphate compounds such as $Cs_3(HSO_4)_2(H_2PO_4)$[12]), are readily reduced upon exposure to H_2, rendering them unsuitable for fuel cell and other electrochemical applications.[13] Accordingly, efforts to expand the chemical space of technologically relevant superprotonic electrolytes remain focused on phosphate materials.

The number of known solid acid phosphate candidates is small. The closest analog to CsH_2PO_4 - RbH_2PO_4 - requires pressures above 1 atm to fully stabilize the cubic, superprotonic phase against dehydration,[14, 15] while substitutions of Cs by Rb and K in CsH_2PO_4 have not yielded technologically valuable materials.[16] The phosphate analogs to $Rb_3H(SeO_4)_2$ - $Rb_3H_3(PO_4)_2$[17] and $Cs_3H_3(PO_4)_2$[18] - do not undergo superprotonic transitions prior to decomposition, even under high steam pressure (though the superprotonic phase may yet be stabilized under high total pressure as is the case in RbH_2PO_4[14, 15]). Furthermore, the compound $Ba_2KH(PO_4)_2$, despite being essentially isostructural to superprotonic $Rb_3H(SeO_4)_2$, does not have particularly high conductivity.[19] While these lines of investigation have not proven fruitful, a recent, promising approach to the development of new phosphate based superprotonic electrolytes based on 'off-stoichiometric' compositions[20] or 'heterogeneous doping'[21] has emerged. Here, one pursues materials in which the cation:polyanion atomic ratio deviates from the canonical values of 1:1 as found in the $x CsHSO_4 – (1-x)CsH_2PO_4$ series of compounds[12, 22-24] and of 3:2 as found in $A_3H(XO_4)_2$ (A = Cs, Rb, NH_4, K; X = S, Se)[11] and $A_3H_3(PO_4)_2$[20] compounds.

Following this approach, we recently reported the phase behavior of the $CsH_2PO_4 – CsH_5(PO_4)_2$ system.[20] Amongst the phases formed in this rich chemical system is the superprotonic

compound $Cs_7(H_4PO_4)(H_2PO_4)_8$, which occurs at a Cs:PO_4 ratio of 7:9 and temperatures between 90 and 190 °C.[25] Rather remarkably, the CsH_2PO_4 and $Cs_7(H_4PO_4)(H_2PO_4)_8$ compounds exhibit eutectoid behavior, forming a non-stoichiometric cubic superprotonic phase of composition stoichiometry $Cs_{1-x}H_{2+x}PO_4$ over a wide range in x.[20] In parallel, Gaydamaka et al. have pursued an analogous study of the RbH_2PO_4 – Rb_2HPO_4 system.[26] These authors have reported that the compound $Rb_5H_7(PO_4)_4$, with a cation:polyanion ratio of 5:4, undergoes a superprotonic transition at ~237° C at which the conductivity rises from ~10^{-5} to ~10^{-2} S/cm, and the activation energy for proton transport becomes ~0.9 eV.[27] Materials with intermediate compositions between RbH_2PO_4 and $Rb_5H_7(PO_4)_4$ were furthermore shown to display enhanced conductivity over that of the end-members. To date, the structure of the high conductivity phase of $Rb_5H_7(PO_4)_4$ has not been reported, nor have the materials at intermediate composition been fully characterized.

The present study was undertaken with the objective of clarifying the phase behavior in the (1-x) RbH_2PO_4 – x Rb_2HPO_4 system in the chemical space from RbH_2PO_4 (x = 0) to $Rb_5H_7(PO_4)_4$ (x = ¼). Using a combination of thermal analysis, in situ x-ray powder diffraction, and impedance spectroscopy, we firmly establish bulk superprotonic conductivity in this system, distinct from the influence of heterogeneous, secondary phases. We find that, across the entire chemical space, the superprotonic phase is cubic. This cubic phase displays variable stoichiometry, best described by the formula $RbH_{2-3y}(PO_4)_{1-y}$ with y reaching at least 0.2 and has the surprising capacity to host vacancies on its polyanion sites.

Methods

Three precursor compounds were synthesized and used for studies in the RbH_2PO_4-$Rb_5H_7(PO_4)_4$ system. The first, tetragonal RbH_2PO_4 (rubidium dihydrogen phosphate, or RDP), was prepared through methanol-induced precipitation from stoichiometric aqueous solutions of the precursors H_3PO_4 and Rb_2CO_3. The second, the compound Rb_2HPO_4•$2H_2O$, was prepared through evaporation-induced precipitation from stoichiometric aqueous solutions of H_3PO_4 and Rb_2CO_3. The synthesis of the third, $Rb_5H_7(PO_4)_4$, was achieved through a high humidity precipitation route using RbH_2PO_4 and Rb_2HPO_4•$2H_2O$ as the reagents. Stoichiometric quantities of these two phosphates were placed in a quartz boat and the mixture was heated in a furnace to 105°C. A steam partial pressure (pH_2O) of 0.83 atm was introduced at this temperature, at which condition

the reagents deliquesced. Precipitation of $Rb_5H_7(PO_4)_4$ was then induced by heating the solution to 130°C under dry N_2. The RbH_2PO_4 and $Rb_5H_7(PO_4)_4$ compounds, used in the subsequent study of phase behavior, were stored at 85°C to prevent absorption of water from the environment. Characterization was performed on materials of global composition $Rb_{1+x}H_{2-x}PO_4$, prepared by mixing stoichiometric quantities of the RbH_2PO_4 (x = 0) and $Rb_5H_7(PO_4)_4$ (x = ¼) precursors. As RbH_2PO_4 has been reported upon extensively in the literature, it was not evaluated in any depth here.

Simultaneous thermal analysis (STA) was carried out using a differential scanning calorimeter/thermogravimetric analyzer (DSC/TGA) Netzsch STA 449F3. Twelve compositions (x = 0.020, 0.026, 0.034, 0.0625, 0.083, 0.110, 0.125, 0.143, 0.167, 0.182, 0.220, and ¼, with an uncertainty in x of ~ 0.003) were examined. For each measurement, a finely ground sample, 40 mg in mass, was lightly compacted into a Pt sample pan. Samples were heated at 1 °C/min to 350 °C, initially under dry Ar (93 sccm). At 130 °C, samples were held at this temperature for two hours and then 8.1 g/h of water vapor, used to achieve pH_2O = 0.7 atm, was introduced to the system.

High temperature (in situ) powder X-ray diffraction (HTXRD) patterns were collected from 135 to 249 °C using a Smartlab 9 kW Gen 3 instrument equipped with an Anton Paar XRK 900 furnace. After combining precursors and grinding, the prepared samples were placed into the sample holder of the XRK 900 furnace and spun during measurement. Humidified gas was introduced at 135°C using a heated, humidified N_2 gas line to achieve pH_2O = 0.83 atm. Data were collected at 35°C intervals from 25 °C to 135 °C with a 10°C/min heating rate between measurements. From 135°C to 235°C, the sample was heated at a rate of 5 °C/min and data were collected at 25°C intervals. At higher temperatures, from 235 °C to 249 °C, the sample was heated at a rate of 2 °C/min and data were collected at 2 °C intervals. Measurements were made of five compositions (x = 0.125, 0.150, 0.180, 0.200, 0.250), supplemented with some limited studies of RbH_2PO_4 (x = 0). For the x = ¼ end-member, the humidity was increased to pH_2O = 0.88 atm upon reaching 180 °C. Comparisons to the thermal results indicated the true temperatures within the XRK 900 furnace were approximately 5 °C higher than the set values, with a spatial variation across the sample of similar magnitude. The estimated true (average) temperatures are reported hereafter. Diffraction patterns were analyzed using the Rietveld

method in the GSAS-II program with the background, sample displacement, lattice parameters, and phase fractions refined.[28] Instrument profile parameters were fixed to values measured independently using the standard, lanthanum hexaboride. Structural models for the known stoichiometric compounds RbH_2PO_4(monoclinic)[29] and $Rb_5H_7(PO_4)_4$[30] were employed without refinement of atomic parameters. The refinement strategy employed for the newly discovered cubic phase is described below alongside the structure descriptions.

Conductivity was measured for the composition $x = 0.180$ by impedance spectroscopy. The sample was formed into a pellet with a diameter of 14.85±0.03 mm and density of approximately 97% of theoretical, under a two-step uniaxial pressing protocol in which the material was pressed at 49 kPa for five min then 98 kPa for an additional five min. The surfaces of the resulting pellet were sanded using 1200 and 2000 grit sandpaper to ensure smoothness; the final pellet thickness was 0.92±0.03 mm. Platinum electrodes, 15 nm in thickness, were sputtered onto either side using a Denton Desktop Sputter IV. Impedance data were collected over the temperature range 70 to 244 °C using an 4284A Agilent LCR analyzer over a frequency range of 0.1 to 10^6 Hz and a voltage amplitude of 20 mV. Between 70 and 130 °C, the sample environment was exposed to a dry N_2 gas stream (40 sccm); between 130 and 180 °C, the gas stream was humidified to 0.83 atm pH_2O; and above 180 °C, the atmosphere was increased to 0.88 pH_2O (balance N_2). The total flow rate was kept constant throughout the experiment. Data were collected in 10 °C intervals between 70 and 180 °C using a heating rate of 5 °C/min between measurements. Data between 180 and 244 °C were collected at 5-10 °C intervals with a heating rate of 2 °C/min between steps. At each measurement condition, samples were allowed to equilibrate for 30 mins before recording the impedance spectrum. The impedance data were analyzed using the commercial software package ZView.

As is the norm for crystallographic studies, all estimated uncertainties are reported in parentheses and reflect the uncertainty in the final digit(s) of the quoted values.

Results and Discussion

Phase Behavior

The (1-x)RbH_2PO_4 – xRb_2HPO_4 phase diagram ($0 \leq x \leq 0.25$) shown in Figure 1 was determined on the basis of the thermal analysis and diffraction measurements. Though $Rb_5H_7(PO_4)_4$ was used in material preparation, for notational ease, Rb_2HPO_4 (the anhydrous product of heating Rb_2HPO_4•$2H_2O$ to the temperatures of reported in Figure 1) is specified as the end member compound of the phase diagram theanhydrous. At temperatures between 125 and 241 °C, the stoichiometric compound $Rb_5H_7(PO_4)_4$ was found to coexist with stoichiometric, monoclinic RbH_2PO_4 (space group $P2_1/m$), as demonstrated in the representative diffraction patterns for several compositions collected at (or close to) 235 °C, Figure S1. Tetragonal RbH_2PO_4 transforms to the monoclinic phase at ~109 °C[31] and is thus not represented in the phase diagram of Figure 1. Gaydamaka reported a similar co-existence of $Rb_5H_7(PO_4)_4$ and RbH_2PO_4 phases, without reactions between the two, for x = 0.1 and 0.2 global compositions, albeit with RbH_2PO_4 in the tetragonal form due to the ambient temperature measurement.[26] The mutual insolubility of $Rb_5H_7(PO_4)_4$ and RbH_2PO_4 is evident from the insensitivity of the high temperature unit cell volumes of these materials to the presence of the other phase (Figure S2, Table S1-S3).

Eutectoid Reaction and Formation of α-RbH_2PO_4

Upon heating, $Rb_5H_7(PO_4)_4$ and RbH_2PO_4(m) were found to undergo a reaction at 242 °C, reflected, for example, in the DSC/TGA profiles of the representative compositions x = 0.026 and 0.182 (pH_2O = 0.7 atm), Figure 2. Though the reaction is followed closely by mass loss, the reaction itself precedes any mass change. Shown on the phase diagram of Figure 1 are the reaction temperatures determined from the 12 discrete x values, with the corresponding DSC/TGA profiles reported in Figure S3. In each case, a thermal anomaly is detected that precedes mass loss. Excluding the end-member composition x = ¼, the anomaly occurs at 242.0(5) °C. We attribute the thermal event to a eutectoid, solid state reaction between $Rb_5H_7(PO_4)_4$ and RbH_2PO_4(m) to form a solid product phase.

The nature of the phase that appeared at 242 °C was established from the *in situ* diffraction studies. Shown in Figure 3 and Figure 4 are representative sets of diffraction patterns for the x = 0.200 and x = 0.180 compositions, respectively. The complete sets of patterns for these

compositions (all measurement temperatures) are shown in Figure S4, with refined cell parameters and phase fractions reported in Tables S4 and S5. As indicated in Figure 1, these representative compositions lie on either side of the eutectoid composition, identified below as occurring at $x \approx 0.190$.

The diffraction measurement of the hypereutectic composition ($x = 0.200$),Figure 3, shows that the two-phase mixture of stoichiometric $Rb_5H_7(PO_4)_4$ and RbH_2PO_4(m) indicate in the phase diagram, Figure 1, is retained to a temperature of 241 °C. At 247 °C (the next temperature at which data were recorded for this composition), the pattern changes markedly, indicative of the phase transformation detected by thermal analysis. At 249 °C all peaks can be indexed to a primitive cubic cell with lattice constant 4.702(1) Å, with no remaining peaks from either precursor.

In the case of the hypoeutectoid composition ($x = 0.180$), Figure 4, analogous behavior is observed. The phases $Rb_5H_7(PO_4)_4$ and RbH_2PO_4(m) are retained to 235 °C (the highest measurement temperature below the eutectoid transition). At 245 °C, the pattern is dominated by a primitive cubic phase, and at 249 °C, all peaks can be indexed to this cell. The cubic lattice at this composition is 4.7138(2) Å (at 249 °C). Rather remarkably, the new cubic phase, as revealed by Rietveld refinement, is isostructural to superprotonic CsH_2PO_4 (sp. grp. $Pm\bar{3}m$). This nonstoichiometric phase, with global composition $Rb_{1+x}H_{2-x}PO_4$, is hereafter referred to as α-RDP. The phase diagram, Figure 1, provides a summary of the diffraction results. No phases other than those indicated were observed under any condition examined.

Beyond revealing the occurrence of a solid state reaction at 242 °C, the thermal measurements showed consistency with a eutectoid composition of $x \geq 0.14$. The measured enthalpy of the eutectoid transition (deconvoluted from the dehydration enthalpy by peak fitting, Figure S5) generally increased as x increased over the range from 0.020 to 0.143, Figure 5, rising from 1.5 kJ/mol to 11.7 kJ/mol, where the enthalpy values have been normalized to the moles of $Rb_{1+x}H_{2-x}PO_4$. The increase occurs because the fraction of material undergoing the transformation monotonically increases as x approaches $x_{eutectoid}$. In the range $0.14 < x < 0.22$ the overlap between the eutectoid transition and dehydration events was too severe to permit accurate measurement of the eutectoid transition enthalpy (see Figure 2b for example). Accordingly, data

collected at higher x values are omitted from Figure 5. Extrapolation to x = 0.180-0.200 suggests an enthalpy of reaction of ≈ 15-16 kJ/mol($Rb_{1+x}H_{2-x}PO_4$).

Heating of the (1-x)RbH_2PO_4 – xRb_2HPO_4 materials in the thermal analysis experiments to even just a few degrees beyond the eutectoid temperature resulted in mass loss, which was accompanied by a thermal signature, as in the example of the x = 0.182 composition, Figure 2b. The initiation of dehydration shifted slightly to lower temperatures with increasing x, from 249.2 °C at x = 0.020 to 244.9 °C at x = ¼ under pH_2O = 0.7 atm (Figure S2). Thus, α-RDP exists only over a narrow temperature window, even at very high H_2O partial pressure. It is known that stoichiometric RbH_2PO_4 cannot be stabilized in the superprotonic cubic structure at any H_2O pressure below 1 atm.[31] Hence, it is not surprising that α-RDP would undergo ready dehydration.

At temperatures between the eutectoid and the solvus temperatures, the diffraction patterns of the hypoeutectoid compositions generally revealed the presence of the two expected phases – RbH_2PO_4(m) and α-RDP. Analysis of the phase fractions in these regions enabled further narrowing of the range for the eutectoid composition. Specifically, at x = 0.180 and T = 245 °C (Figure 4b), Rietveld refinement revealed the mass percentage of α-RDP to be 96.3(5) %. Application of the phase rule and an assumption of stoichiometric $Rb_5H_7(PO_4)_4$, imply the α-RDP phase to have a composition of x = 0.1868(9), and thus $x_{eutectoid}$ must exceed this value. Due to temperature variations across the sample stage, the phase behavior in the hypereutectic region could not be fully discerned on the basis of the diffraction data alone. Despite some uncertainty in the temperature, the behavior of the x = 0.200 composition sets an upper bound for the eutectoid composition. Specifically, at a nominal temperature of 247 °C (Figure 3b), Rietveld refinement revealed the mass percentage of α-RDP in the mixture with $Rb_5H_7(PO_4)_4$ to be 64.77(4) %. In turn, this implies the α-RbH_2PO_4 phase occurring here to have a composition of x = 0.194(1). Thus, the eutectoid composition, x_{euc}, is limited to $0.187 < x_{euc} < 0.194$ and is taken hereafter to be at the center of this range, with value 0.190(4).

Properties of the End-Member Compounds and the Solvus Lines

The thermal behavior of the end-member material, $Rb_5H_7(PO_4)_4$ (x = ¼), showed slight but important differences from those of the intermediate compositions, Figure 6a. A large thermal

event was observed for this material at 243.2 °C, slightly higher than the mean eutectoid temperature of 242 ±0.5 °C. Furthermore, the enthalpy for this event was found to be 13.4 kJ/mol(α-RDP), larger than the maximum value of 11.7 kJ/mol recorded at $x = 0.143$ (Figure 5). These factors suggest a stoichiometric transition of $Rb_5H_7(PO_4)_4$ into α-RDP, similar to what has been observed for the transition of $Cs_7(H_4PO_4)(H_2PO_4)_8$ into α-CDP.[20, 25] The diffraction data (reported in full in Figure S6 and Table S6) revealed a simple cubic pattern at 249 °C with cell parameter 4.7028(5) Å, Figure 6c, consistent with the occurrence of α-RDP and with the proposed phase diagram. However, the $Rb_5H_7(PO_4)_4$ phase appeared to be retained up to 247 °C, Figure 6b. While the possibility that this reflects a true feature of the material system (which is treated here as binary system despite the chemical complexity) cannot be entirely ruled out, we assign the observation of $Rb_5H_7(PO_4)_4$ at temperatures beyond the stoichiometric transition temperature of 243 °C to cold spots in the heating stage. Additionally, slow kinetics due to poor heat transfer between loosely contacted particles (in contrast to the light compaction employed for the thermal analysis) may have contributed to a sluggish transformation. On the basis of conductivity measurements (but no crystallographic studies), Gaydamaka reported a superprotonic transition at 237 °C in $Rb_5H_7(PO_4)_4$[27], consistent with the structural transition proposed here.

With the stoichiometric transition temperature for $Rb_5H_7(PO_4)_4$ so estimated, the solvus line in the hypereutectoid region is taken to be linear between this transition and the eutectoid position. Similarly, in the hypoeuctectoid region, the solvus line is taken to be linear between the eutectoid point and the superprotonic transition of stoichiometric RbH_2PO_4. The latter is ≈ 280 °C, as measured by thermal analysis by both Gaydamaka[26] (onset at 255 °C, peak at 283 °C) and Li[31] (peak at 276 °C).[31] In both studies, despite kinetic competition from dehydration, the polymorphic transition to cubic RDP was reliably detected. Attempts to evaluate the solvus line by application of the phase rule to diffraction patterns collected in the two-phase region were unsuccessful due to the sensitivity of the results to the slight variations in the stage temperature and, at temperatures well above the eutectoid transition, due to the ready dehydration of the material.

Structure of α-RDP

The global composition of α-RDP, with a Rb/PO_4 ratio > 1, appears at first glance, to be incompatible with the superprotonic CsH_2PO_4 structure type (sp. grp. $Pm\bar{3}m$), in which Cs atoms adopt a simple-cubic arrangement and the polyanion units occupy the cube center positions.[32, 33] This structure, a derivative of the CsCl structure, does not have interstitial sites of sufficient size and appropriate coordination environment to host large alkali atom species and thus accommodate the Rb excess in α-RDP. For example, possible sites at (½ ,½, 0), and (¼, ¼, ¼) have cations in the nearest neighbor coordination sphere. Furthermore, if Rb excess were to be accommodated by Rb interstitials, one would expect the cell parameter to increase with *x*. The observation here, however, is a decrease in cell parameter in α-RDP from an estimated value of 4.837(12) Å for the hypothetical stoichiometric material (Figure S7) to an average of 4.706 ± 0.006 Å across the three compositions of finite *x* (and *T* = 249 °C). As an alternative to Rb interstitial incorporation, one can consider the formation of $Rb \leftrightarrow PO_4$ antisite defects, in which Rb cations replace H_2PO_4 anions as a means of accommodating the Rb excess in α-RDP. While not inconsistent with the cell contraction, cation/anion antisite defects carry an extremely large electrostatic energy penalty in an ionic material, even with next nearest phosphate groups serving as the sites from which protons are lost to achieve overall charge balance. Accordingly, antisite defects are unlikely to be the means by which the nonstoichiometry is realized. With these possibilities eliminated, we suggest that the material achieves Rb excess by hosting vacancies on the anion sites. Here, the overall charge balance is maintained by removal of additional protons from other H_2PO_4 groups. In this scenario, the chemical formula of the cubic phase is described as $RbH_{2-3y}(PO_4)_{1-y}$ rather than by the global composition of $Rb_{1+x}H_{2-x}PO_4$. The cell contraction then reflects the loss of large anion groups and local contraction about the anion vacancies.

Shown in Figure 7 is the structure of α-RDP at *x* = 0.18 and 245 °C, corresponding to the refinement presented in Figure 4b. Associated crystallographic results are summarized in Table 1. The structure of cubic CsH_2PO_4 was used as a starting model in the analysis and the following steps were taken in the refinement. The lattice parameter and isotropic displacement parameters for the Rb and P atoms were allowed to vary freely. The isotropic displacement parameter for O was then set to a value 7% larger than that of P, in analogy to the properties of cubic CsH_2PO_4,[33] and the oxygen position refined with a restraint targeting a P-O bond length of 1.53 Å.

Additionally, as alluded to above, a small amount of RbH_2PO_4(m) was detected in this pattern (< 4 wt. %), and the relative amounts of the two phases was freely refined. As with the lower temperature refinements, the instrument profile parameters were fixed at the reference values obtained from a measurement of LaB_6, whereas the sample displacement was freely varied. In all cases in which the α-RDP phase was detected, the diffraction peaks from this material were slightly broadened relative to those of the other phases. This feature was treated by refining the α-RDP crystalline size. Peak broadening is plausibly explained by the presence of anion vacancies which would give rise to a distribution in interatomic distances. The final refinement statistics for the refinement indicated in Figure 4b, R_{wp} = 6.24% and GooF = 7.56, along with the overall features of the difference pattern, indicate the satisfactory nature of the model. The final R_F (R_{Bragg}) for the α-RDP phase was 7.89%. The model captures the diffraction features of the x = 0.200 composition at 249° C (Figure 3c) particularly well.

Similar to stoichiometric cubic CsH_2PO_4, the polyanion groups at the unit cell center of α-RDP can adopt one of several different orientations, and an example of one possible orientation is shown in Figure 7b. In the stoichiometric material, the mean oxygen site occupancy is 1/6, and this has been interpreted to correspond to six possible orientations.[3] For the material α-RDP with x = 0.18, 15 % of the anion sites are vacant according to the proposed structural interpretation, implying an oxygen site occupancy of 0.14. Given the limited number of diffraction peaks and the possibility of poor powder randomization due to crystallite coarsening on heating, refinement of the P and O site occupancies to confirm the hypothesis of anion site vacancies was not possible. Instead, the occupancies were fixed in the Rietveld analysis at the values expected for the proposed structural model and ignoring the small impact on α-RDP stoichiometry of the presence of residual RbH_2PO_4(m) in this pattern. Refinements at higher temperatures, at which RbH_2PO_4(m) was completely consumed but the diffraction data were slightly obscured by a higher background signal, produced similar results, Table S5. In the case of the end member compound $Rb_5H_7(PO_4)_4$, stoichiometric transformation to α-RDP implies, rather remarkably, that the structure is stable with as much as 20% of the polyanion sites unoccupied.

Superprotonic Conductivity

The conductivity of the $Rb_{1+x}H_{2-x}PO_4$ material with x = 0.18 (near the eutectoid composition) increased sharply between 230 and 238 °C, rising by over two orders of magnitude across this

narrow temperature window, Figure 8. The behavior is directly evident in the raw impedance spectra (Figure S8). While there is a slight offset from the transition temperature of 241 °C measured by thermal analysis, the increase in conductivity is consistent with the proposed eutectoid transition to superprotonic α-RDP. At the highest temperature of measurement, 244°C, the conductivity is 6×10^{-3} S/cm, similar to that estimated for stoichiometric RbH_2PO_4 (7×10^{-3} S/cm), Figure S9, and somewhat lower than that of CsH_2PO_4 (2×10^{-2} S/cm) at a comparable temperature.[16] As is typical of superprotonic transformations,[21] the reverse transition to the low conductivity state was sluggish on cooling. Here, the reverse reaction involves disproportionation into the two precursor phases, a process that presumably adds to the commonly observed hysteresis. The conductivity of the metastable state displayed linear behavior in an Arrhenius plot between 230 and 244°C, from which the activation energy, E_a, and preexponential factor ln(A) for proton transport in the expression $\sigma = \frac{A}{T} exp\left(\frac{E_a}{k_b T}\right)$ (where T is temperature and k_b is Boltzmann's constant) were obtained. The resulting values are 0.57 eV and 13.84 S/cm K, respectively, both larger than the corresponding terms in CsH_2PO_4 (0.384 eV and 11.32 S/cm K).[16] Thus, over the narrow temperature range of stability of α-RDP, the higher activation energy overwhelms the benefits of a higher preexponential factor and results in a lower conductivity than that of CsH_2PO_4.

Discussion

Observation of a phase isostructural to superprotonic CsH_2PO_4 with a large concentration of phosphate group vacancies is surprising, but fully supported by the experimental results. In particular, the diffraction data reveal the transformation of all compositions near the eutectoid to a cubic phase at temperatures just beyond the thermal anomaly at 242 -243°C. The cell contraction relative to stoichiometric cubic RbH_2PO_4 eliminates all other possible structural configurations. The superprotonic transitions reported by Gaydamaka et al. across the RbH_2PO_4 – Rb_2HPO_4 system[26] can be understood to reflect the formation of α-RDP.

It is of some value to evaluate the thermal and entropic signatures of the transition to α-RDP. The eutectoid reaction (at $x = 0.190(4)$ and T = 242.0(5) °C) can be written as

$$0.203\ RbH_2PO_4 + 0.159\ Rb_5H_7(PO_4)_4 \rightarrow \alpha\text{-}RbH_{1.52}(PO_4)_{0.84} \quad (1)$$

from which it evident that 80 mole % of the Rb species in the product derive from $Rb_5H_7(PO_4)_4$, implying the reaction thermodynamics are dominated by this reactant. From the estimated enthalpy of this reaction of 15.5 kJ/mol(α-RDP) noted above, the entropy of reaction is 30.1 J/mol-K.

In the case of the end member compound, the stoichiometric reaction (at T = 243.2 °C) is

$$0.2\ Rb_5H_7(PO_4)_4 \rightarrow \alpha\text{-}RbH_{1.4}(PO_4)_{0.8} \quad (2)$$

The enthalpy recorded for this transition, 13.4 kJ/mol, is taken to be a lower bound for the true value due to the overlap with dehydration (as noted for compositions in the range $0.14 < x < 0.22$). The corresponding transition entropy is 26.0 J/mol-K, and again reflects a minimum value. Both the enthalpy and entropy changes associated with the reactions to form α-RDP are greater than those of stoichiometric CsH_2PO_4, 11.3 kJ/mole and 22.5 J/mol-K, respectively. Because the structures of the low temperature phases differ, monoclinic CsH_2PO_4 vs. orthorhombic $Rb_5H_7(PO_4)_4$ and indeed the hydrogen positions in the latter are not known[30], it is not possible to readily identify the sources of the differences. However, due to the presence of anion vacancies, α-RDP would be expected to have greater configurational entropy than stoichiometric, cubic CDP, and hence a larger entropy of transition to α-RDP is reasonable.

The presence of phosphate group vacancies, while stabilizing the cubic structure, might be expected to negatively influence the conductivity due to the loss of proton transport pathways relative to the stoichiometric analog. On the other hand, the lower conductivity of α-RDP, higher activation energy for proton transport, and larger pre-exponential factor are all consistent with what is observed in cubic CDP upon Rb doping, in which the hydrogen bond network is grossly unchanged relative to stoichiometric, cubic CDP.[16] Thus, the specific reasons for the slightly lower conductivity of α-RDP remain to be isolated.

Summary and Conclusions

The phase behavior of in the (1-x) RbH_2PO_4 – x Rb_2HPO_4 system in the chemical space from RbH_2PO_4 (x = 0) to $Rb_5H_7(PO_4)_4$ (x = ¼) has been carried out by *in situ* XRD and thermal analysis under controlled atmospheres with high steam partial pressure to suppress dehydration. The system was found to display eutectoid behavior, with a eutectoid composition of x = 0.190(5) and transition temperature of 242.0(5) °C. Above the transition temperature, the

structure adopts the cubic superprotonic structure of CsH_2PO_4, though with a large concentration (~15%) of polyanion vacancies, denoted here as α-RDP. Charge balance is maintained by a concomitant reduction in the number of protons on remaining polyanion groups. The conductivity of the material of eutectic composition approaches that of superprotonic CsH_2PO_4. The end-member compound $Rb_5H_7(PO_4)_4$ appears to undergo a stoichiometric transition to α-RDP with a remarkable 20% polyanion vacancies. The thermal stability window of α-RDP is small, rending this material unlikely to be of direct technological value. However, the surprising discovery of an off-stoichiometric superprotonic cubic phase in which cations outnumber polyanions indicates that non-stoichiometry holds promise for continued material discovery.

Supporting Information

Selected diffraction patterns; cell volumes as functions of temperature; complete DSC/TGA data; estimation of cell parameter of hypothetical cubic RbH_2PO_4 at ambient pressure; selected impedance spectra.

Acknowledgements

Financial support has been provided by the National Science Foundation (DMR-1807234, DMR-2118201 and DGE-1842165). This work made use of the J.B. Cohen X-Ray Diffraction facility at Northwestern University, supported by the NSF MRSEC program (NSF DMR-1720139). We thank Elise Goldfine for assistance with diffraction measurements.

Tables

Table 1. Fractional atomic coordinates and displacement parameters of α-$Rb_{1+x}H_{2-x}PO_4$ at x = 0.180 and T = 245 °C. Structure adopts space group $Pm\bar{3}m$ with a = 4.7138(2) Å. The P-O bond distance is 1.51(2) Å. Numbers in parentheses reflect the uncertainty in the final digit(s) of the quoted values.

Atom	x	y	z	site	occupancy[a]	U_{iso} (Å^2)
Rb	0	0	0	1*a*	1	2.42(4)
P	½	½	½	1*b*	0.85	1.91(6)
O	½	0.203(1)	0.375(2)	24*l*	0.14	2.05(6)[b]

[a] fixed to match global chemistry

[b] tied to the U_{iso} of P by a multiplicative factor of 1.073

Figure Captions

Figure 1. Phase diagram across the (1-x) RbH_2PO_4 – x Rb_2HPO_4 system for $0 \leq x \leq 0.25$. Datapoints indicated with parentheses are in slight disagreement with the proposed phase boundaries, likely due to cold spots in the high-temperature XRD stage. The eutectoid transition temperature, established by thermal analysis, occurs at 242.0 ± 0.5 °C, and the eutectoid composition is $x = 0.190 \pm 0.004$. The eutectoid transition occurs at a significantly lower temperature than the superprotonic transition of stoichiometric RbH_2PO_4 (≈ 280° C[26, 31]).

Figure 2. DSC/TGA measurements of materials with composition (a) $x = 0.026$, and (b) $x = 0.182$, both under $pH_2O = 0.7$ atm. In both cases, the first thermal event in the DSC signal occurs without any mass loss. Events at higher temperature align with mass loss seen in the TG signal and are accordingly attributed to dehydration.

Figure 3. Diffraction patterns and Rietveld refinements for $x = 0.200$ at (a) 241 °C, below the eutectoid transition, (b) 247 °C, just above the eutectoid transition, and (c) 249 °C, within the single-phase cubic region, all collected under $pH_2O = 0.83$ atm.

Figure 4. Diffraction patterns and Rietveld refinements for $x = 0.180$ at (a) 235 °C, below the eutectoid transition, (b) 245 °C, just above the eutectoid transition, and (c) 249 °C, within the single-phase cubic region, all collected under $pH_2O = 0.83$ atm.

Figure 5. Enthalpy of the eutectoid transition as a function of composition.

Figure 6. High temperature phase transition of $Rb_5H_7(PO_4)_4$ ($x = ¼$) revealed (a) by thermal analysis under $pH_2O = 0.7$ atm; and by x-ray diffraction patterns collected at (b) 237°C and (c) 249°C under $pH_2O = 0.88$ atm.

Figure 7. Proposed structure of α-RDP at x near the eutectoid composition ($x = 0.180$) with (a) all 24 oxygen sites shown; and (b) four oxygen sites that form one of the tetrahedral group orientations shown.

Figure 8. Conductivity of α-RDP at x near the eutectoid composition ($x = 0.180$) as measured over the temperature range of 25°C to 244°C. The jump in conductivity corresponds to the superprotonic phase transition observed in DSC and high temperature XRD measurements.

References

1. A. Baranov, *Crystallography Reports*, 2003, **48**, 1012-1037.
2. D. A. Boysen, T. Uda, C. R. I. Chisholm and S. M. Haile, *Science*, 2004, **303**, 68.
3. S. M. Haile, C. R. I. Chisholm, K. Sasaki, D. A. Boysen and T. Uda, *Faraday Discussions*, 2007, **134**, 17-39.
4. K. Imamura and J. Kubota, *Sustain. Energ. Fuels*, 2019, **3**, 1406-1417.
5. J. Otomo, S. Nishida, H. Takahashi and H. Nagamoto, *Journal of Electroanalytical Chemistry*, 2008, **615**, 84-90.
6. A. B. Papandrew, C. R. I. Chisholm, R. A. Elgammal, M. M. Ozer and S. K. Zecevic, *Chemistry of Materials*, 2011, **23**, 1659-1667.
7. O. Paschos, J. Kunze, U. Stimming and F. Maglia, *Journal of Physics-Condensed Matter*, 2011, **23**.
8. T. Uda, D. A. Boysen, C. R. I. Chisholm and S. M. Haile, *Electrochemical and Solid State Letters*, 2006, **9**, A261-A264.
9. T. Uda and S. M. Haile, *Electrochemical and Solid State Letters*, 2005, **8**, A245-A246.
10. A. Baranov, L. Shuvalov and N. Shchagina, *JETP Letters*, 1982, **36**, 459-462.
11. A. Pawlowski, C. Pawlaczyk and B. Hilczer, *Solid State Ionics*, 1990, **44**, 17-19.
12. S. M. Haile, G. Lentz, K. D. Kreuer and J. Maier, *Solid State Ionics*, 1995, **77**, 128-134.
13. R. B. Merle, C. R. I. Chisholm, D. A. Boysen and S. M. Haile, *Energy Fuels*, 2003, **17**, 210-215.
14. D. A. Boysen, S. M. Haile, H. J. Liu and R. A. Secco, *Chemistry of Materials*, 2004, **16**, 693-697.
15. C. E. Botez, R. J. Tackett, J. D. Hermosillo, J. Z. Zhang, Y. S. Zhao and L. P. Wang, *Solid State Ionics*, 2012, **213**, 58-62.
16. A. Ikeda, D. A. Kitchaev and S. M. Haile, *Journal of Materials Chemistry A*, 2014, **2**, 204-214.
17. S. Sanghvi and S. M. Haile, *Journal of Solid State Chemistry*, 2021, **296**.
18. S. Sanghvi and S. M. Haile, *Solid State Ionics*, 2020, **349**.
19. C. R. I. Chisholm, E. S. Toberer, M. W. Louie and S. M. Haile, *Chemistry of Materials*, 2010, **22**, 1186-1194.
20. L. S. Wang, S. V. Patel, E. Truong, Y.-Y. Hu and S. M. Haile, *Chemistry of Materials*, 2022, **34**, 1809-1820.
21. V. G. Ponomareva and I. N. Bagryantseva, *Solid State Ionics*, 2019, **329**, 90-94.
22. V. G. Ponomareva and I. N. Bagryantseva, *Inorg. Mater.*, 2012, **48**, 187-194.
23. Y. Yamane, K. Yamada and K. Inoue, *Solid State Ionics*, 2008, **179**, 483-488.
24. C. R. I. Chisholm, Ph.D., California Institute of Technology, 2003.
25. L. S. Wang, S. V. Patel, S. S. Sanghvi, Y. Y. Hu and S. M. Haile, *Journal of the American Chemical Society*, 2020, **142**, 19992-20001.
26. A. A. Gaydamaka, V. G. Ponomareva and I. N. Bagryantseva, *Solid State Ionics*, 2019, **329**, 124-130.
27. A. A. Gaydamaka, V. G. Ponomareva and I. N. Bagryantseva, *Ionics*, 2019, **25**, 551-557.
28. B. H. Toby and R. B. Von Dreele, *Journal of Applied Crystallography*, 2013, **46**, 544-549.

29. M. T. Averbuch-Pouchot and A. Durif, *Acta Crystallographica*, 1985, **C41**, 665-667.
30. M. T. Averbuch-Pouchot and A. Durif, *Acta Crystallographica* 1985, **C41**, 1555–1556.
31. Z. K. Li and T. B. Tang, *Mater. Res. Bull.*, 2010, **45**, 1909-1915.
32. C. E. Botez, J. D. Hermosillo, J. Zhang, J. Qian, Y. Zhao, J. Majzlan, R. R. Chianelli and C. Pantea, *The Journal of Chemical Physics*, 2007, **127**, 194701.
33. K. Yamada, T. Sagara, Y. Yamane, H. Ohki and T. Okuda, *Solid State Ionics*, 2004, **175**, 557-562.

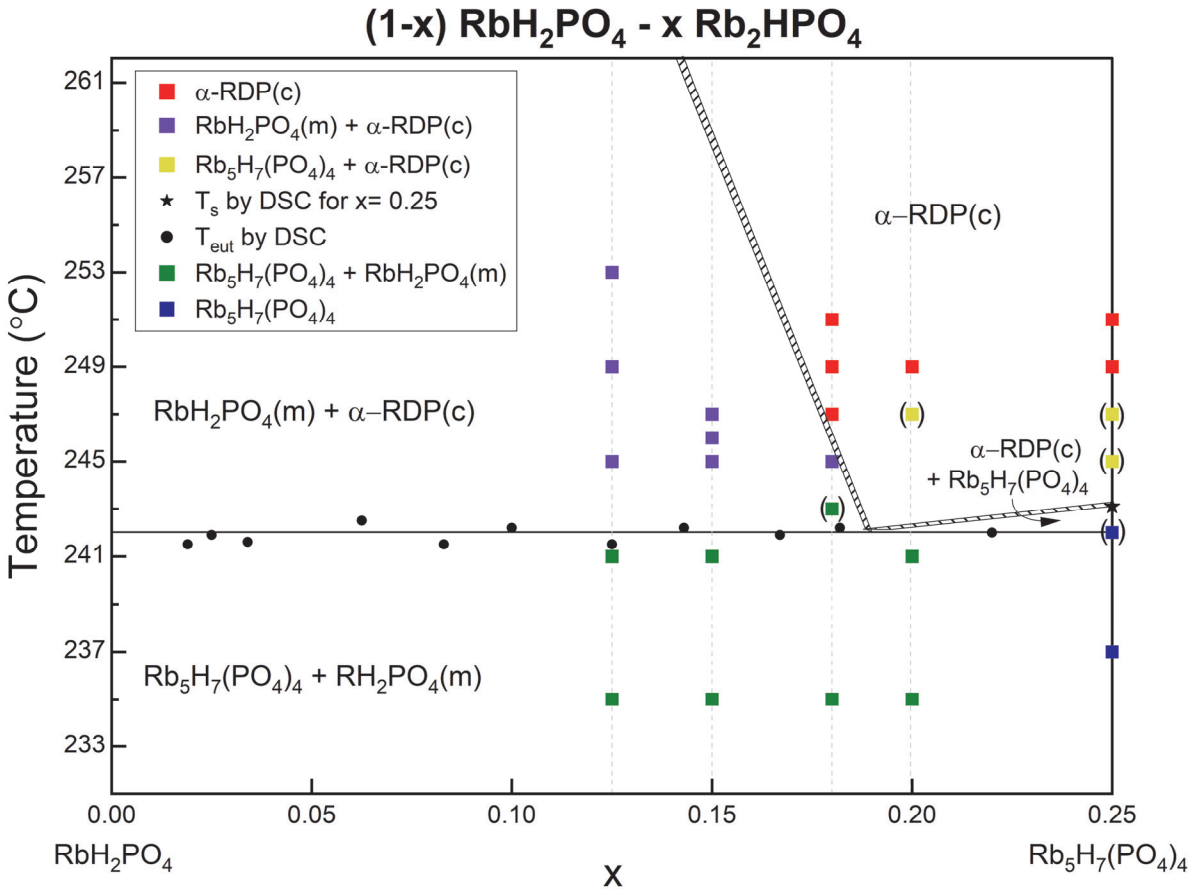
(1-x) RbH2PO4 - x Rb2HPO4
α-RDP(c)
RbH2PO4(m) + α-RDP(c)
Rb5H7(PO4)4 + α-RDP(c)
Ts by DSC for x= 0.25
Teut by DSC
Rb5H7(PO4)4 + RbH2PO4(m)
Rb5H7(PO4)4
α–RDP(c)
RbH2PO4(m) + α–RDP(c)
α–RDP(c) + Rb5H7(PO4)4
Rb5H7(PO4)4 + RH2PO4(m)
Temperature (°C)
261
257
253
249
245
241
237
233
0.00
0.05
0.10
0.15
0.20
0.25
RbH2PO4
Rb5H7(PO4)4
x

Figure 1.

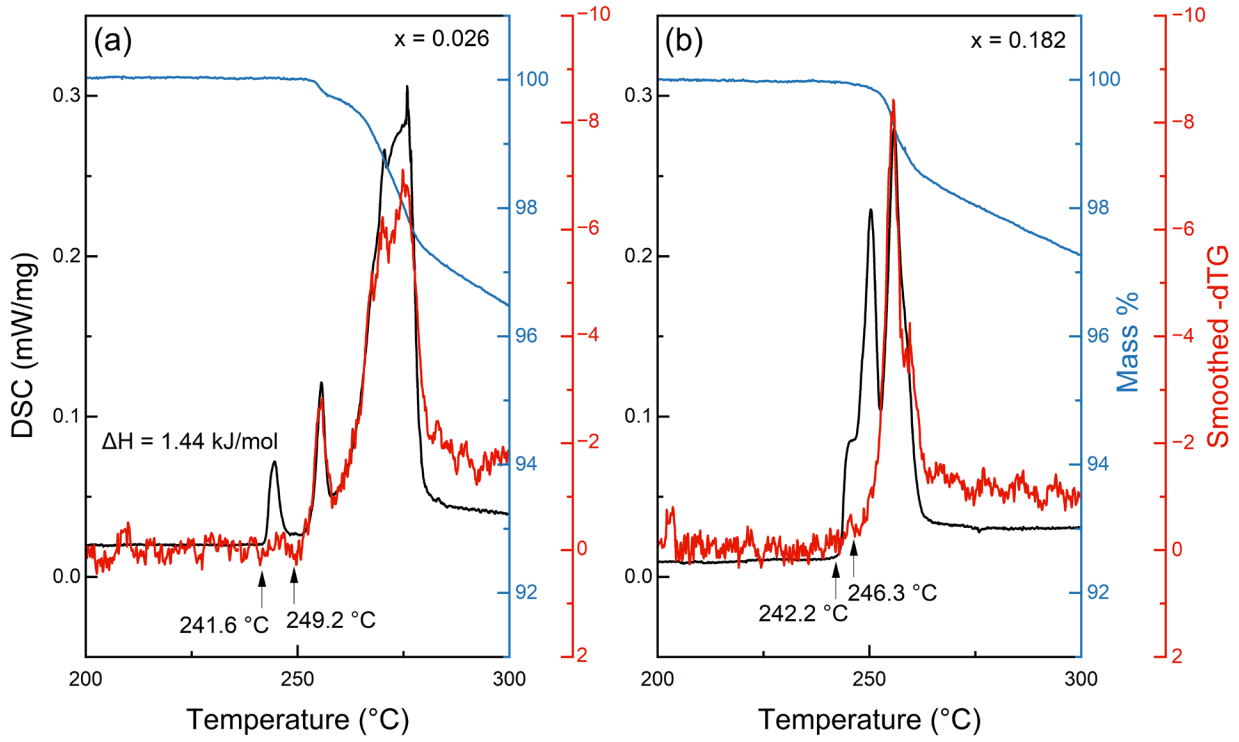
(a)
x = 0.026
ΔH = 1.44 kJ/mol
241.6 °C
249.2 °C
(b)
x = 0.182
242.2 °C
246.3 °C
DSC (mW/mg)
Mass %
Smoothed -dTG
Temperature (°C)
Temperature (°C)

Figure 2.

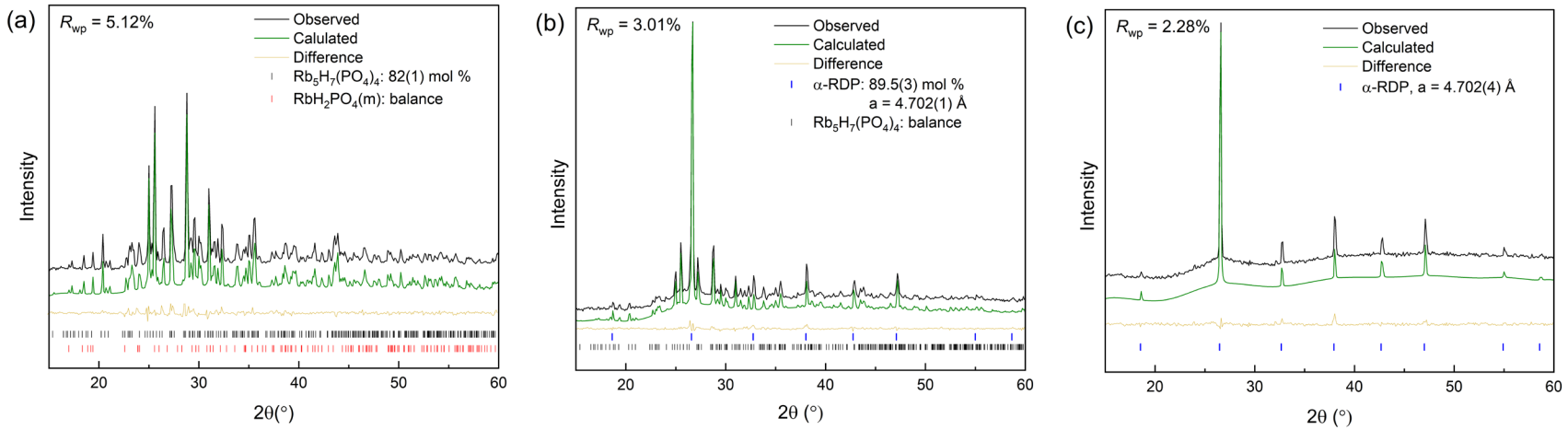

Figure 3.

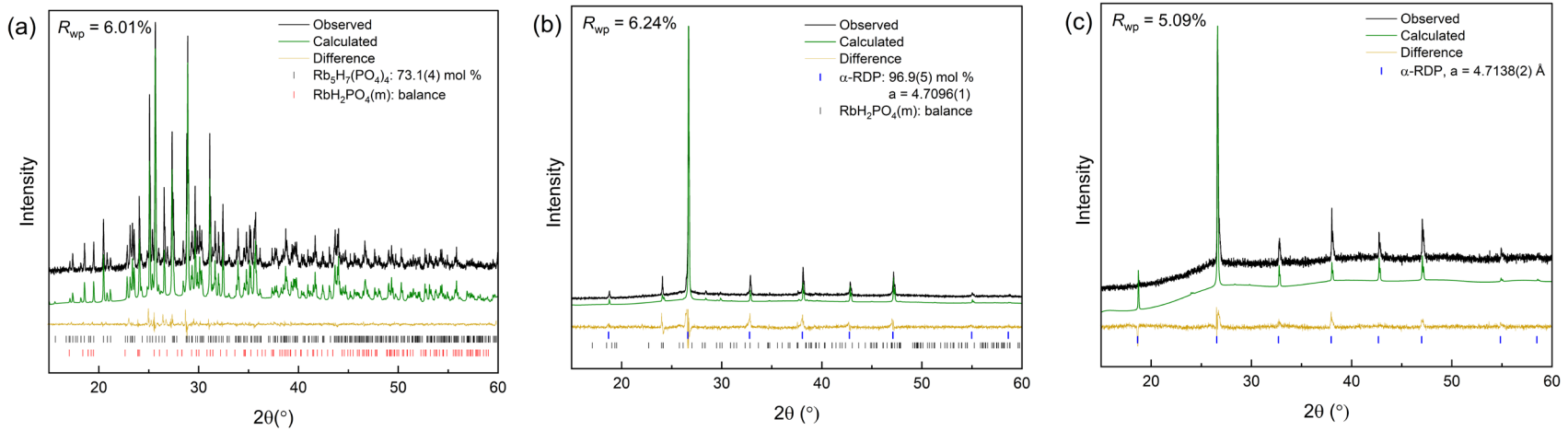

Figure 4

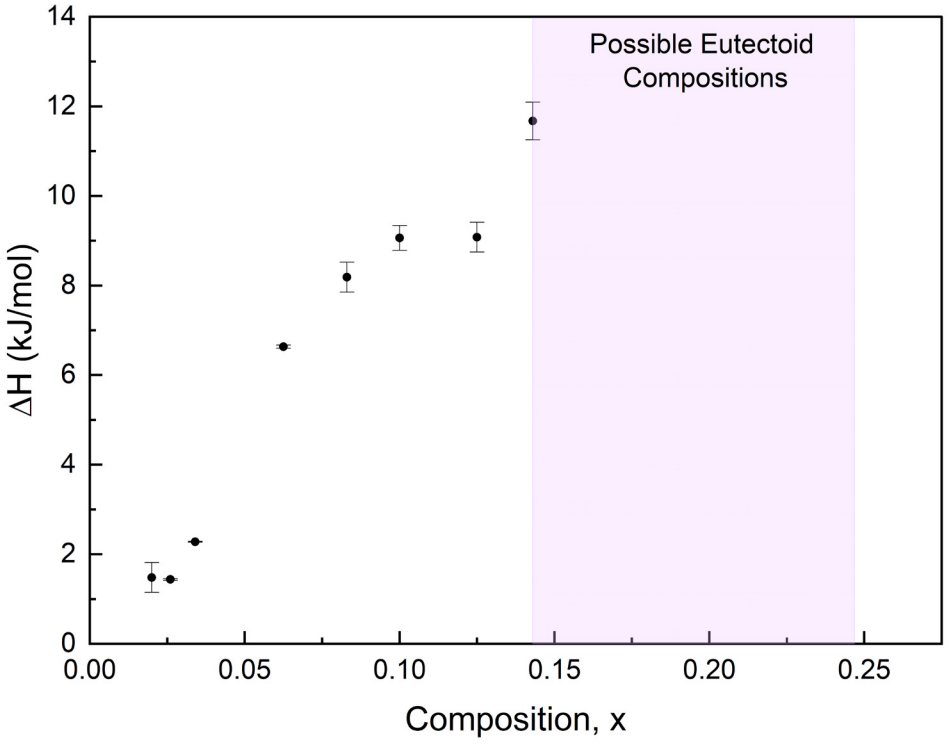
Possible Eutectoid
Compositions
ΔH (kJ/mol)
Composition, x
0
2
4
6
8
10
12
14
0.00
0.05
0.10
0.15
0.20
0.25

Figure 5.

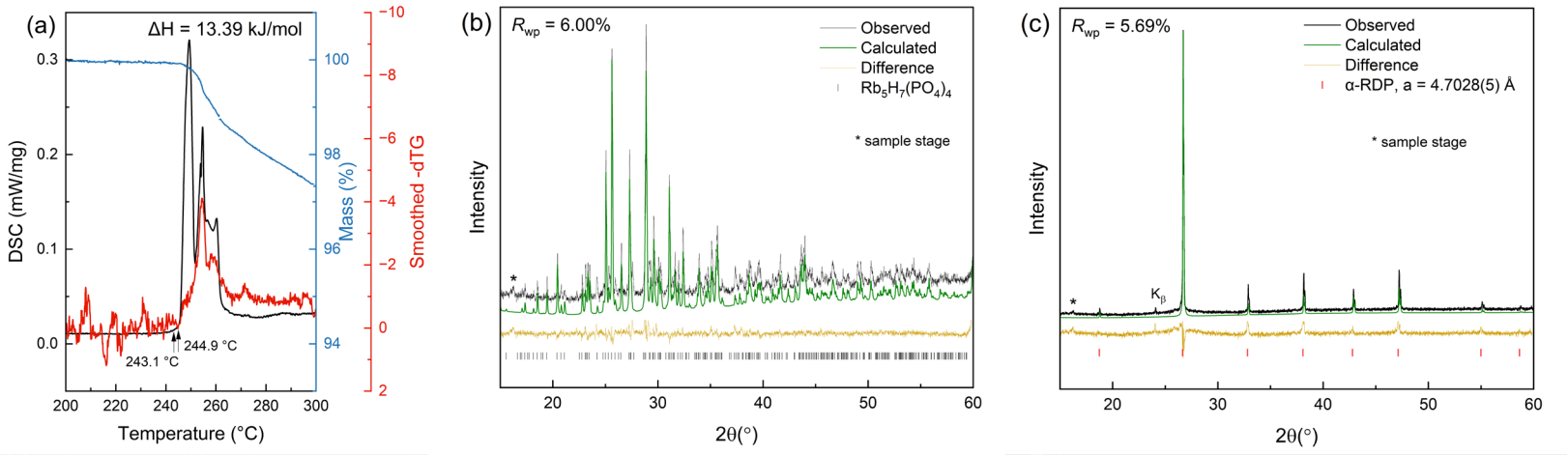
(a)
ΔH = 13.39 kJ/mol
DSC (mW/mg)
Mass (%)
Smoothed -dTG
243.1 °C
244.9 °C
Temperature (°C)
(b)
R_{wp} = 6.00%
Observed
Calculated
Difference
$Rb_5H_7(PO_4)_4$
* sample stage
Intensity
2θ(°)
(c)
R_{wp} = 5.69%
Observed
Calculated
Difference
α-RDP, a = 4.7028(5) Å
* sample stage
K_β
Intensity
2θ(°)

Figure 6

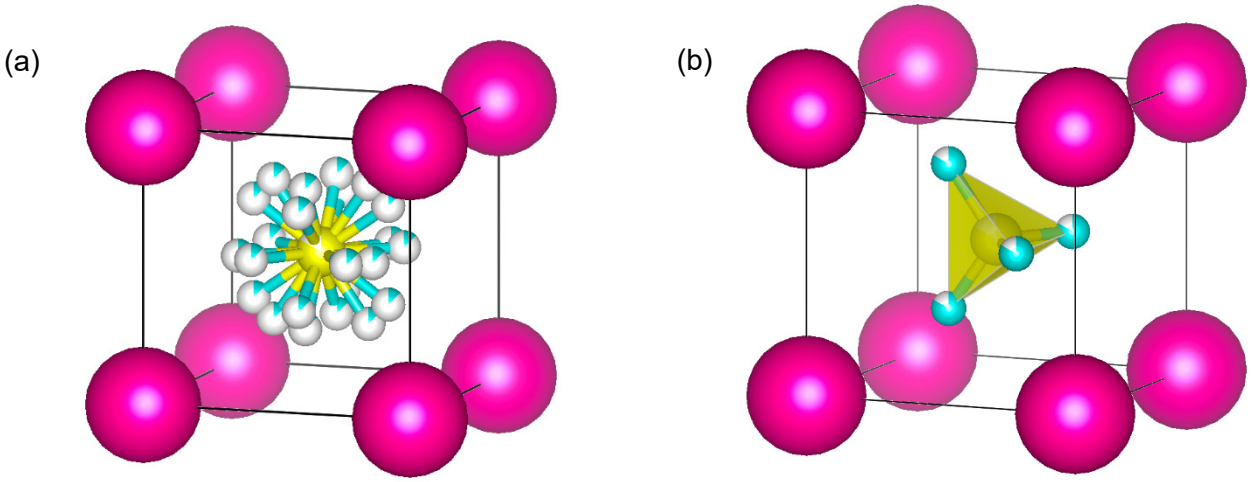

Figure 7

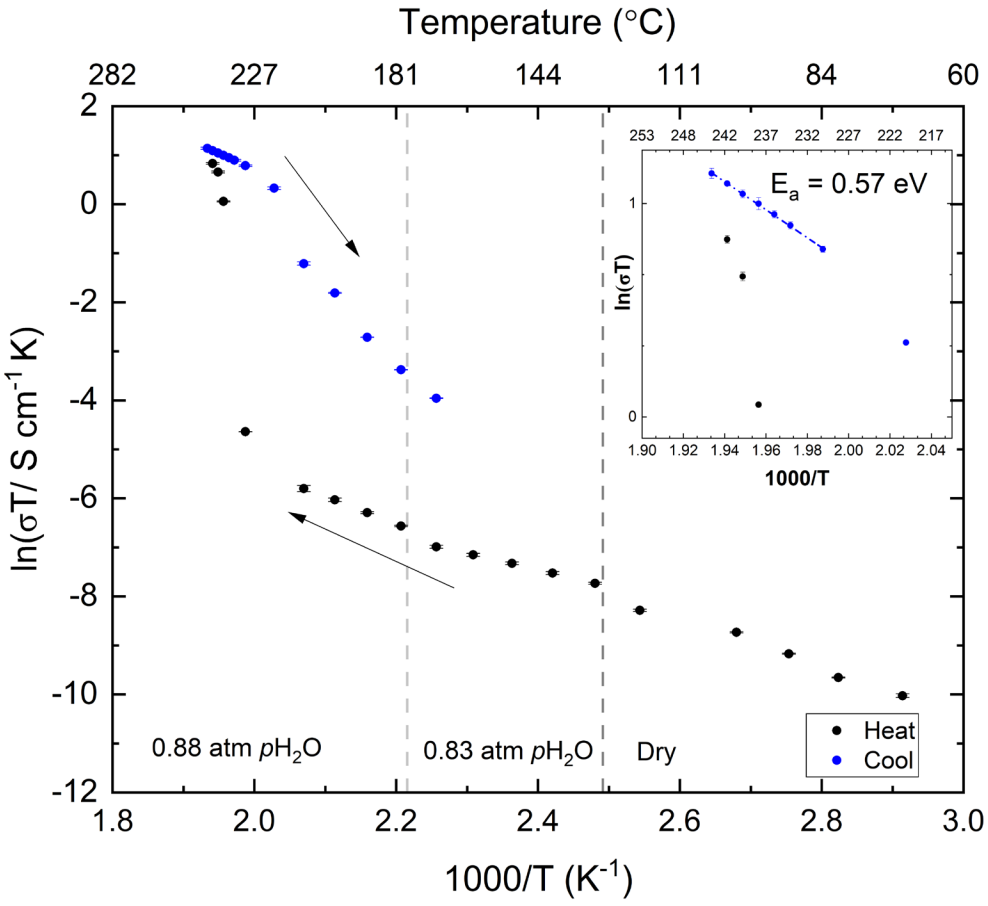

Figure 8.